A planar model for mass flows impacting obstacles

Maria Paula Cabuya & Miguel Angel Cabrera
Universidad de los Andes, Bogotá, Colombia

ma.cabrera140@uniandes.edu.co

Abstract

Mass flows are a common process in mountain environments, posing a risk to its inhabitants and their infrastructure. An alternative to mitigate such impacts is the construction of mitigation structures, like rigid or flexible barriers. This work presents the design of a planar setup for the study of the filling mechanism of mass flows when impacting a rigid and a flexible barrier. In a planar setup, the channel has a width slightly greater than one particle wide, allowing the observation of a two-dimensional mass flow. The planar setup provides a vantage look into the internal kinematics at impact, allowing the characterization of the evolution of the stagnant zone. Preliminary tests review the effect of the barrier height in the evolution of the stagnant zone, splitting the filling process into a surge sequence controlled by the length of the stagnant zone. Moreover, the filling capacity is found to be controlled by the barrier stiffness, implying an advantage in the use of flexible structures. The experimental setup provides an opportunity for the validation of numerical frameworks considering the interaction of mass flows against obstacles.

1 INTRODUCTION

Mountain communities deal with the occurrence of several types of mass movements (Hungr et al. 2014), which magnitude can be accentuated or its frequency increased under extreme weather conditions. For example, after the warm phase of the ENSO period of 2010–2011, Colombia faced economic losses up to US$222 million due to road closure by landslides (MinTransporte 2014). An alternative to mitigate such impacts is the construction of mitigation structures, like rigid or flexible barriers. These barriers are designed to limit the runout of mass movements like landslides, rock falls, and debris flows, and withhold the impact while preserving its serviceability. The mass movement impact forces can be computed as a function of the movement height and velocity, the particle size distribution, the presence of fluid, and the topographic features at the structure location (e.g., terrain slope, channel cross-section, channel length) (Wendeler 2016).

Two main approaches have been proposed, considering either the hydrostatic pressure or the kinetic energy of the impacting mass (Armanini 1997). These formulations have been compared with experimental observations in large scale and laboratory-scale experiments (Nagl et al. 2019, Scheidl et al. 2013, Wendeler et al. 2019) while facing several challenges in identifying the process controlling features and linking them with observations in the field. Scaling of the particle-fluid interactions or the obstacle stiffness is particularly challenging in reduced scale experiments, demanding a meticulous experiment design. Moreover, the impact of a mass flow against an obstacle is a complex three-dimensional process, occurring predominantly in the flow direction, but presenting secondary flows that change along the obstacle width (Leonardi et al. 2015, Proske et al. 2018). The material filling behind the obstacle consists of a flowing layer above of a stagnant-zone, also called dead-zone (see Fig. 1). The rate at which the stagnant-zone evolves behind the obstacle allows the distinction of two filling mechanisms. These mechanisms are the run-up or pile-up mechanism characterized by an accelerating or a decelerating impinging flow, respectively. The kinematics on both mechanisms are yet to be understood, requiring detailed insight into the mass flow at impact as recently presented by Sanvitale et al. (2019). An alternative for gaining such observational insight is the planar configuration, where a channel with a width slightly greater than one particle wide allows the observation of the mass movement (Pinzon and Cabrera 2019). This setup provides an experimental alternative to the two-dimensional numerical simulations presented by Faug et al. (2009).

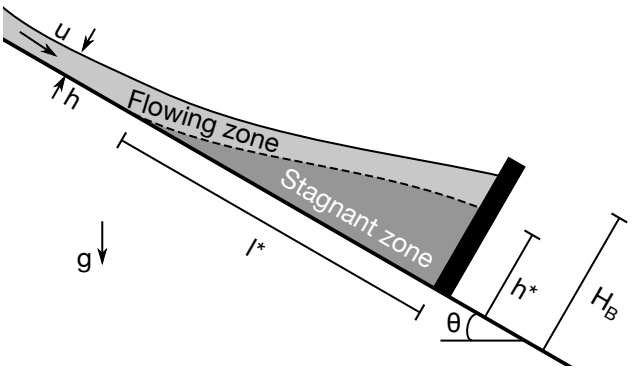

Figure 1: Schematic of the impact and filling mechanism of a granular flow against a barrier. The stagnant zone propagates upwards, with dimensions h^* and l^*, until reaching the barrier height H_B.

In this work, we present the design and first tests of a planar setup for the study of mass flows impacting a rigid and a flexible barrier. The experimental setup is described in Sec. 2, the experimental results are presented and discussed in Sec. 3, and the main conclusions and recommendations for further work are presented in Sec. 4.

2 SCALE MODEL

The planar setup consists of two 1.5 m$\times$1.1 m PMMA windows, enclosing an inner aluminium sheet. The aluminium sheet is 1.25 mm thick with an inner slope of 30° and 1.33 m long, from the release area (see Fig. 2). The bed over which the particles flow is smooth, with the micro-roughness resultant from the laser cutter over the aluminium sheet. Experiments are performed with ceramic beads, manufactured by Sigmund-Lindner GmbH, of 1.0 mm in diameter and a density $\rho_\mathrm{p} = 3600\ \mathrm{kg/m^3}$. Each bead is in contact with the surrounding beads and at most with a side PMMA window, reducing the equivalent confining friction coming from the side-walls.

The purpose of the planar setup is that the aluminium sheet thickness is slightly thicker than one particle diameter, so only one bead can move freely between the PMMA windows and reproduce a nearly two-dimensional space. In this setup we studied two flow scenarios: (i) flows with no obstacle, characterizing the flow conditions; and (ii) flows against a vertical barrier.

The experimental protocol is as follows: First,

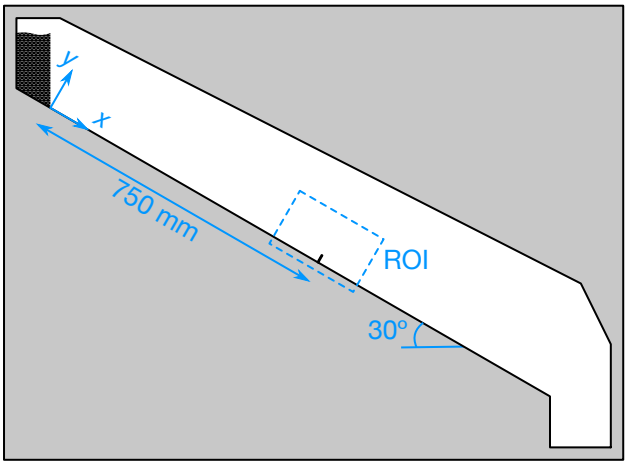

Figure 2: Experimental model in a planar configuration, with a cantilever barrier located at 750 mm from release. The Region of Interest (ROI) focuses at the barrier location and records the back-lighted image of the flowing particles. Note that the channel width is nearly 1.2 times the particle diameter.

the ceramic beads are deposited in a column of 100 mm×227 mm, on top of the model (see Fig. 2). The beads are released by the simultaneous displacement of a side gate connected to two pneumatic actuators along the z-axis. After release, the beads flow down the slope until reaching the barrier or the container at the end of the slope. At a distance of nearly 750 mm, the flow is back-lighted by a led panel and is recorded on the opposite side by a high-speed camera at a frame rate of 800 fps. The back-lighted recordings have a resolution of 640×400 pixels and are analysed with the spatio-temporal technique described in Cabrera and Wu (2016) and the Particle Image Velocimetry open-source algorithm PIVlab developed by Thielicke and Stamhuis (2014).

In the study of flows impacting a vertical barrier, we explore variations in the barrier stiffness by changing its material and height. Two barrier types are studied: a rigid barrier made of PMMA sheet (Young modulus $E = 2100$ MPa (Diacrilicos 2019)), and a flexible barrier made of cork sheet ($E = 5$ MPa (Bernacork 2011)). Both barriers are 1 mm thick. Three barrier heights are studied $H_B = [10, 20, 40]$ mm, all in a cantilever condition, fixed at its base and normal to the channel bed.

3 RESULTS AND DISCUSSION

3.1 Flow characterization

The granular flow of ceramic beads within the planar setup is explored without the presence of a barrier and at a distance of 750 mm from release. First, an initially dilute flow arrives with an average velocity of 2.76 mm/s, followed by a dense flow with a constant and continuous flow height of 6 mm and flow velocity of 0.16 m/s. These observations lead to a Froude number

$$\mathrm{Fr} = \frac{\bar{u_x}}{\sqrt{gh\cos\theta}} = 0.23 \quad (1)$$

and an Inertial number

$$\mathrm{I} = \frac{5\bar{u_x}d}{h^{3/2}\sqrt{2g\cos\theta}} = 1.3\times10^{-2}, \quad (2)$$

where $\bar{u}$, h, d, θ, and g are the depth averaged flow velocity, flow height, particle diameter, slope angle, and earth's gravitational acceleration, respectively (see Fig. 1). Both dimensionless quantities allow the characterization of the observed flows within the regime of dense granular flows, as described by MiDi (2004), and set the reference conditions for the flow impact against a barrier.

3.2 Flow impact and filling mechanism

The flows against the barrier occur similarly as in the characterization experiments with an incoming dilute flow, followed by a continuous dense flow. Figure 3(a) and 3(b) presents the impact sequence of ceramic beads against a 10 mm high rigid barrier and flexible barrier, respectively. Overall, the difference between both barriers is the flow thickness behind the obstacle and the number of particles that overflow. The scenario with a rigid barrier shows a steeper stagnant zone while the scenario with a flexible barrier shows little overflow. Moreover, the rigid barrier captures material above its height H_B, implying a greater catching volume than the flexible case. However, lesser overflow is observed in the experiments with a flexible barrier. This greater trapping potential of the flexible barrier is observed to be independent of the barrier height, and can be attributed to greater damping at impact. This damping at impact sets an upwards-propagating shockwave that stabilizes the incoming particles, reducing the overall barrier overflow when compared with its rigid equivalent.

After impact, a stagnant zone forms behind the obstacle, expanding with a relative height h^* and relative length l^* (see Fig. 1). The evolution of h^* and l^* are measured employing the Spatio-temporal image analysis, allowing the identification of stagnant particles in the recorded frames and along a pixel line next to the obstacle (along the y-axis) and next to the channel bed (along the x-axis), respectively.

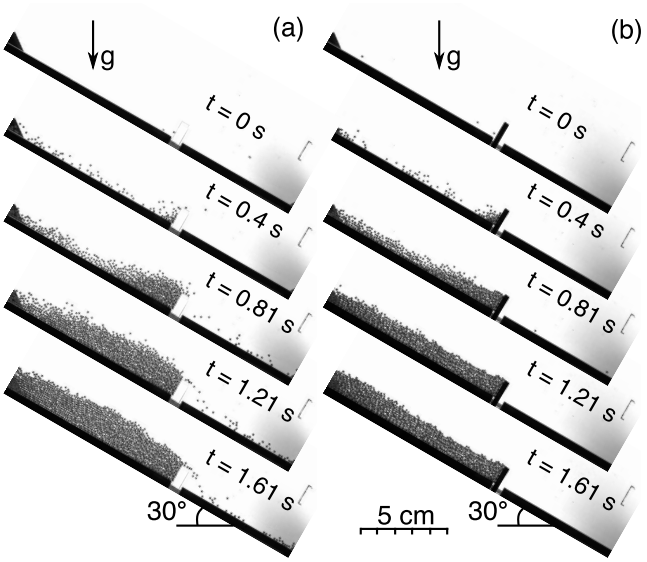

Figure 3: Impact sequence of ceramic beads against a 10 mm high barrier. (a) rigid barrier and (b) flexible barrier.

The temporal evolution of h^* and l^* is presented in Fig. 4. The rate of h^* shows a split of the filling process into two sequences for $H_B \geq 20d$. This split is not observed in the evolution of l^*, implying that the tangential propagation of the stagnant zone is continuous and controls the supply of material that reaches the obstacle and increases h^*. This supply of material can remain continuous for $H_B = 10d$ but is interrupted at greater barrier heights. Moreover, the evolution of h^* and l^* grows at a constant rate, of ≈10 mm/s and ≈20 mm/s, respectively. Unfortunately, l^* extends outside the ROI available, being not possible to define its final extension when $h^* = H_B$. Note that in all experiments, the barriers were overflown, with a lesser amount in the experiments with a flexible barrier.

The initiation times of both h^* and l^* differ, requiring greater times for the identification of l^* in all cases. This difference might result from the measuring method that requires the formation of a consistent pattern along the y-axis. Nevertheless, the pattern identification provides a comprehensive description of the filling process for both rigid and flexible barriers and suggest to be considered separately.

Despite the small size of both particles and experimental setup, it was possible to measure deflections on the flexible barriers, increasing with the barrier height H_B, peaking at 0.4°, 1.2°, and 1.6°, respectively. It is considered that this deflection results from the material height behind the barrier, rather than from the velocity of the flowing layer, and the decrease in the barrier flexural stiffness when increasing its height. Moreover, it supports the argument of the potential damping at impact that reduces the kinematics of the flowing particles.

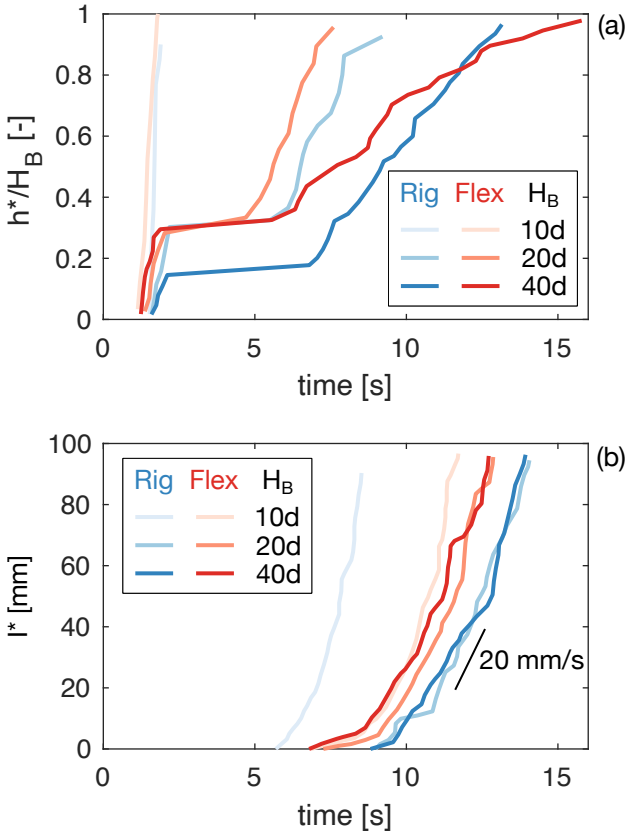

Figure 4: Temporal evolution of (a) the relative height h^* and (b) relative length l^* of the stagnant zone behind the barrier. Blue and red lines correspond to experiments with a rigid barrier and a flexible barrier, respectively.

4 CONCLUSIONS AND FURTHER WORK

This work presented a planar setup for the study of granular flows and its impact mechanisms against a rigid and a flexible barrier. The planar setup provides a valuable look of the internal kinematics at impact, allowing the direct measurement of the evolution of the stagnant and flowing zones behind the barrier. The setup is first tested without a barrier, and the observed flows fall within the regime of dense granular flows. The experiments with a barrier depicted a filling mechanism mainly controlled by the barrier height H_B. For barrier heights $H_B \geq 20d$, the evolution of the relative filling height h^* splits in two, being controlled by the propagation of the stagnant zone length l^*. This relation provides an insight into the mechanism that controls the evolution of the stagnant zone behind an obstacle, where the upwards propagation prevails. Overall, flexible barriers presented a lesser overflown than rigid barriers, showing signs of greater damping as in the case of

deflections up to 1.6°.

Ongoing work focuses on the characterization of the kinematics of the filling mechanisms and the role of the slope angle. Next steps on this experimental setup are the incorporation of fluid and mounting it in a geotechnical centrifuge to increase the flow inertia, hence increasing the impact kinematics.

ACKNOWLEDGMENTS

The research leading to these results received funding from the Patrimonio Autonomo Fondo Nacional de Financiamiento para la Ciencia, la Tecnología y la Innovación Francisco José de Caldas under grant agreement No. 164-2019. The authors would like to thank J. Monroy, J. Acosta, and M. Tobar, from Universidad de los Andes, for their assistance during the model setup and instrumentation.

REFERENCES

Armanini, A. (1997). On the dynamic impact of debris flows. In *Recent developments on debris flows*, pp. 208–226. Springer.

Bernacork (2011). Ficha técnica de aglocork térmico. Technical report, Bernacork.

Cabrera, M. & W. Wu (2016). Space–time digital image analysis for granular flows. *International Journal of Physical Modelling in Geotechnics*.

Diacrilicos (2019). Ficha técnica del acrílico virgen. Technical report, Diacrilicos.

Faug, T., R. Beguin, & B. Chanut (2009). Mean steady granular force on a wall overflowed by free-surface gravity-driven dense flows. *Physical Review E 80*(2), 021305.

Hungr, O., S. Leroueil, & L. Picarelli (2014, Apr). The Varnes classification of landslide types, an update. *Landslides 11*(2), 167–194.

Leonardi, A., F. Wittel, M. Mendoza, R. Vetter, & H. Herrmann (2015). Particle-fluid-structure interaction for debris flow impact on flexible barriers. *Computer-Aided Civil and Infrastructure Engineering (accepted)*, in press.

MiDi, G. (2004). On dense granular flows. *The European Physical Journal E 14*(4), 341–365.

MinTransporte (2014). Plan vías-cc: vías compatibles con el clima. Technical report, Ministerio de Transporte de Colombia.

Nagl, G., R. Kaitna, & J. Hübl (2019). Forschungsbauwerk zur untersuchung von murgängen und deren einwirkung auf schutzbauwerke. *ce/papers 3*(2), 161–165.

Pinzon, G. & M. Cabrera (2019, 6). Submerged planar granular column collapse: Fluid fluxes at the collapsing granular front. In *Proceedings of the 7th International Conference on Debris-Flow Hazards Mitigation. In press*.

Proske, D., A. Krawtschuk, O. Zeman, C. Scheidl, & M. Chiari (2018). Debris flow impacts on masonry arch bridges. In *Proceedings of the Institution of Civil Engineers-Bridge Engineering*, Volume 171, pp. 25–36. Thomas Telford Ltd.

Sanvitale, N., E. Bowman, & M. A. Cabrera (2019). Small scale impact on rigid barrier using transparent debris-flow models. In *Association of Environmental and Engineering Geologists; special publication 28*. Colorado School of Mines. Arthur Lakes Library.

Scheidl, C., M. Chiari, R. Kaitna, M. Müllegger, A. Krawtschuk, T. Zimmermann, & D. Proske (2013). Analysing debris-flow impact models, based on a small scale modelling approach. *Surveys in Geophysics 34*(1), 121–140.

Thielicke, W. & E. Stamhuis (2014). Pivlab - towards user-friendly, affordable and accurate digital particle image velocimetry in matlab. *Journal of Open Research Software 2*(e30).

Wendeler, C. (2016). Debris-flow protection systems for mountain torrents. *WSL Berichte. Swiss Federal Institute for Forest, Snow and Landscape Research WSL*.

Wendeler, C., A. Volkwein, B. W. McArdell, & P. Bartelt (2019). Load model for designing flexible steel barriers for debris flow mitigation. *Canadian Geotechnical Journal 56*(6), 893–910.